Available online at www.sciencedirect.com

ScienceDirect

Procedia CIRP 00 (2023) 000–000

www.elsevier.com/locate/procedia

17th CIRP Conference on Intelligent Computation in Manufacturing Engineering

A model for the rapid prediction of small feature width producible by Metal AM

Prospera Sonuo Sibanda[a,b], Michael Ryan[a], Samuel Bigot[a,*]

[a]*Cardiff University School of Engineering, Queen's Buildings 14-17 The Parade, CF24 3AA, United Kingdom.*

[b]*Safran Seats GB, Llantarnam Industrial Park Cwmbran, Torfaen, NP44 3HQ, United Kingdom.*

* Corresponding author. *E-mail address: BigotS@cardiff.ac.uk.*

Abstract

In this paper, an analytical parametric model is presented for the swift prediction of small features producible in the X-Y plane through the Metal AM Laser Powder Bed Fusion (LPBF) process. This model can be employed to design and create surface textures on Additive Manufactured parts without the need for costly post-processing steps. The Rosenthal equation is the basis for the model, which considers both the build parameters of the LPBF process and the thermo-physical properties of the materials. The initial model was constructed and assessed using one LPBF machine followed by the implementation of a tuning method utilizing the Limited Memory Algorithm for Bound Constrained Optimization to enhance the model's accuracy. Overall, the findings suggest that with a simple optimization step based on a single printed tuning sample, precise analytical models can be established for specific LPBF machines and materials combinations.

Peer-review under responsibility of the scientific committee of the 17th CIRP Conference on Intelligent Computation in Manufacturing Engineering, 12-14 July, Gulf of Naples, Italy

Keywords: LPBF; Metal Additive manufacturing; Direct Texturing; Analytical Model, Model Optimisation

1. Introduction

Laser Powder Bed Fusion (LBPF) can create custom-made parts that traditional methods may find challenging or impossible. Direct texturing, which involves printing a designed surface texture, is advantageous for aircraft interior applications because it would eliminats expensive post-processing and could mask the irregularities of LPBF surfaces, improving its visual appeal. CAD and CAM software advancements have simplified 3D model creation and direct texturing using LPBF, but assessing the feasibility of textured designs for specific machine and material combinations is difficult due to uncertainties in achievable geometries and machine limitations. To evaluate feasibility of manufacturing direct texturing designs, it is necessary to understand how minimum texture size can be evaluated pre-manufacture to enable the design of textures sensitive to the machine and material combination.

Previous research has concentrated on experimentally or numerically determining the melt-pool width, with the goal of predicting and improving the dimensional accuracy of LPBF parts [1]–[4]. Although some analytical models have been developed for the prediction of dimensional accuracy, they rely on experimentally- derived melt-pool widths which can be time-consuming and expensive. As a result, there is a lack of methods for quick estimation of achievable small feature sizes at the design stage, particularly in relation to direct texturing and specific machine and material combinations. This research proposes a new method for quickly predicting the width of small features manufactured by LPBF for direct texturing applications.

Peer-review under responsibility of the scientific committee of the 17th CIRP Conference on Intelligent Computation in Manufacturing Engineering, 12-14 July, Gulf of Naples, Italy

2. Review of Melt-Pool Width Estimation

In the LPBF process, a laser beam is used to selectively melt metallic powder in the scanning direction (y), creating a melt-pool. This can be achieved using a Continuous Wave (CW) laser or Pulsed Width Modulation (PWM) laser [5], with the characteristics of the melt-pool influenced by both the thermo-physical properties of the material and the machine's build parameters [3].

Several studies aimed at evaluating the melt-pool width produced by the LPBF process, and for that purpose the Rosenthal equation, originally developed for predicting the thermal history of melt pools in fusion welding, is commonly used by researchers. Due to the similarities between fusion welding and LPBF, authors [1], [2], [3] have applied the Rosenthal equation to LPBF as it provides a simple, accurate, and fast way to estimate melt-pool characteristics like width and shape, in comparison to FEA and experimentation. The simplified Rosenthal equation is shown in equation 1 [1].

$$W_{mp} \approx \sqrt{\frac{8}{\pi e}.\frac{\lambda.P}{\rho.C_p.v(T_m-T_o)}} \quad (1)$$

$Where\ W_{mp}$ is the melt-pool width(m), λ is the absorptivity, P is the laser power (W), e is the natural exponent, ρ is the density of the material($kg.m^{-3}$), C_p is the pecific heat ($J.kg^{-1}.K^{-1}$), v is the laser velocity ($m.s^{-1}$), T_m is the melting temperature (K), T_o is the initial temperature before melting (K).

For the estimation of a melt-pool width in LPBF, the same assumptions were used in this research as used by Promoppatum et al [1].

The following section provides a detailed description of a theoretical parametric model that was developed to rapidly predict the producible small feature widths in the forming direction (x) for different combinations of machines and materials.

3. New Metal AM Feature Width Prediction Model

Metal additive manufacturing typically involves the use of infill and contour laser scan tracks, which are automatically controlled by CAM software to produce the bulk of the component and obtain optimum surface quality, respectively. The parametric model developed in this study considers these dual scanning strategies, but assumes that for small features designed to create surface textures, the infill and contour tracks generated by the CAM software will always be parallel as more complex scanning strategies will be generated only for larger feature sizes. Hence, the generic formula for estimating the theoretical peak width for a combination of contour and infill laser scans can be calculated using equation 2.

$$w_{theo\_p} = \sqrt{\frac{8}{\pi e}.\frac{\lambda.P}{\rho.C_p.v(T_m-T_o)}} + 2(n_c-1)h_c + 2h_{c.i} + (n_i-1)h_i \quad (2)$$

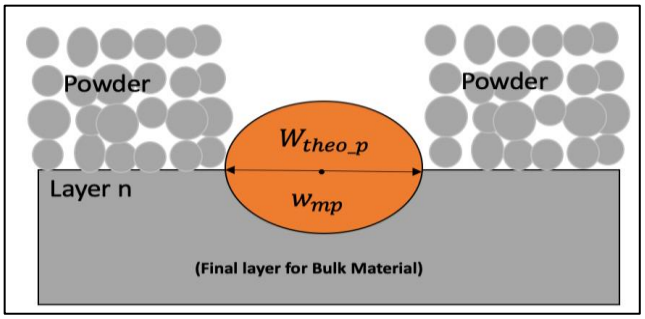

Figure 1. Schematic of Case 1 feature width (X-Z plane)

Where n_c is the number of contour tracks, n_i is the number of infill tracks, h_c is the hatch distance between adjacent contour tracks, h_i is the hatch distance between adjacent infill tracks, $h_{c.i}$ is the hatch distance between adjacent contour and infill tracks and w_{mp} is the melt-pool width that can be calculated based on the material properties and build parameters.

The prediction model focuses on three distinct cases investigated to validate the proposed model, including single and double laser scan tracks, and contouring with one infill scan track. These tests were adequate for an initial evaluation of the analytical model while maintaining the parallel scanning strategy, with the CAM slicing software managed by an external supplier.

3.1. Case 1: Single Laser Track

In Case 1 (Figure 1), a single laser melt track represents the feature, and the minimum feature width is equal to the melt-pool width calculated based on the thermo-physical properties of the material and build parameters of the machine. Assuming that the laser parameters is the same as the infill parameters, the $\boldsymbol{w_{mp} = w_i}$, where $\boldsymbol{w_i}$ is the infill melt-pool width.

The number of contours n_c= 0 and the number of infills, n_i=1, hence by referring to the generic formula, the formula for determining the theoretical peak width for Case 1, single scan track is the same as shown in equation 1.

3.2. Case 2: Double Laser Track

For the double laser scan track scenario (Case 2), the feature is represented, in the CAM, by two laser scan tracks in the scanning direction (Y). This is illustrated in **Figure 2**.

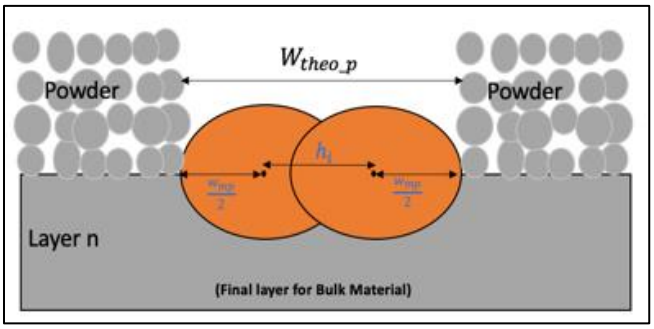

Figure 2.Schematic of Case 2 feature width (X-Z plane)

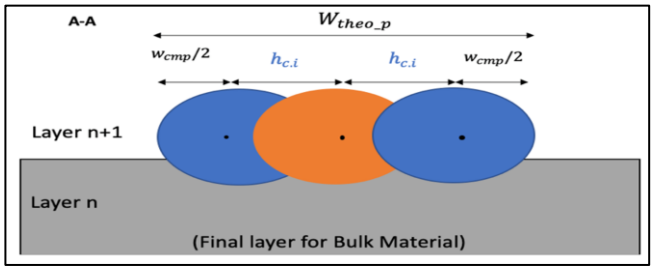

Figure 3. Schematic of Case 3 feature width (X-Z plane)

In Case 2, the feature is represented by two laser scan tracks in the scanning direction and the distance between the scan tracks is determined by the hatch spacing. The melt-pool width $\boldsymbol{w_{mp} = w_i}$. In addition, $\boldsymbol{n_c}$= 0 and $\boldsymbol{n_i}$=2. Hence, by referring to the generic formula (equation 3.3), the formula for determining the theoretical peak width for Case 2 is shown in equation 3.

$$w_{theo\_p} = \left(\sqrt{\frac{8}{\pi e}.\frac{\lambda.P}{\rho.C_p.v(T_m - T_o)}}\right) + h_i \qquad (3)$$

3.3. Case 3: Contouring and Infill Laser Track

For Case 3 (contouring and infill laser track), the feature is represented by a contour scan and an infill laser scan in the scanning direction (Y). To develop the theoretical peak width equation for Case 3 condition, $\boldsymbol{w_{mp} = w_{cmp}}$, where $\boldsymbol{w_{cmp}}$ is the contour melt-pool width. In addition, the number of contours $\boldsymbol{n_c}$= 2 (based on the cross section in the X-Z plane) and the number of infills, $\boldsymbol{n_i}$ =1. Referring to the generic formula, the formula for determining the theoretical peak width for Case 3,contouring and infill laser track is shown in equation 4.

$$w_{theo\_p} = \left(\sqrt{\frac{8}{\pi e}.\frac{\lambda.P}{\rho.C_p.v(T_m - T_o)}}\right) + 2h_{c.i} \qquad (4)$$

4. Validating the new model using parts produced by - LPBF (Continuous Laser)

4.1. Experimental Setup

To assess the precision of the parametric model described earlier (section 3.1-3.3), six AlSi7Mg samples were manufactured using an SLM280 machine, a 700W continuous laser, and a print volume of 280 x 280 x 365 mm. The study focused on four key parameters: laser power, speed, hatch spacing, and build height. The chemical composition of AlSi7Mg is shown in Table 1.

Table 1: Chemical composition in % of AlSi7Mg [6]

Si	Mg	Cu	Ti	Fe	Mn	Zn	Al
6.5-7.5	0.5-0.8	<0.05	<0.3	<0.2	<0.1	<0.1	Bal.

Table 2: Input parameters for the manufacture of samples 1-6 in AlSi7Mg

Sample No.	Strategy	Hatch Power (W)	Contour Power (W)	Hatch Spacing (mm)
1	X	650	350	0.17
2	X	650	350	0.17
3	Y	500	270	0.13
4	Y	500	270	0.13
5	Z	580	310	0.15
6	Z	580	310	0.15

4.2. Variations in Laser Power and Hatch Spacing.

The energy input is expressed in the form of Volumetric Energy Density (VED) and this is used to determine whether the metal powder will sufficiently melt the powder to create a high density part (Galimberti et al., 2016). The VED is calculated using Equation 5 (Tang et al., 2017).

$$VED = \frac{P}{v.\ h_s.t} \qquad (5)$$

Where VED is Volumetric Energy Density, Jmm^{-3}, P is laser power, W, v is laser speed, mms^{-1}, h_s is hatch spacing in mm and t is the layer thickness is mm.

To ensure a stable AM process and stay within appropriate processing windows of the materials used while adopting the Rosenthal equation, the VED was kept constant while evaluating the effect of variations in build parameters on the model accuracy. This was achieved by maintaining a constant scanning speed of $2100mms^{-1}$ and $600mms^{-1}$ for the hatch and contour scans respectively, and finding suitable laser power and hatch spacing settings to keep the VED within a targeted range using Magics software. Three build strategies were used (X, Y, and Z) with similar VEDs but different combinations of laser power and hatch spacing. Sample manufacturing was done using these strategies with each strategy applied to fabricate two samples, resulting in a total of six samples. All six samples were manufactured by applying the strategies in Table 2, with each strategy applied to fabricate two samples. Hence the Default Strategy X, Strategy Y and Strategy Z were applied to Sample number 1, 2; Sample 3, 4; and Sample 5, 6 respectively.

4.3. Variation in Feature Size and Build Position.

The feature design is composed of six rectangular extrusions with heights varying from 0.1mm to 0.3mm in increments of 0.1mm. The process parameters from Table 3 4, as well as the powder thermophysical properties, were utilized to calculate the theoretical feature widths for Case 1, Case 2, and Case 3. Using CATIA V5 software, the samples were designed with dimensions of 30x15x4mm (LxWxH), with Figure 3 10 illustrating the CAD design for Sample 1, including section views with feature widths of 0.3mm (Case 1), 0.47mm (Case 2), and 0.66mm (Case 3). Figure 4 shows the CAD Design.

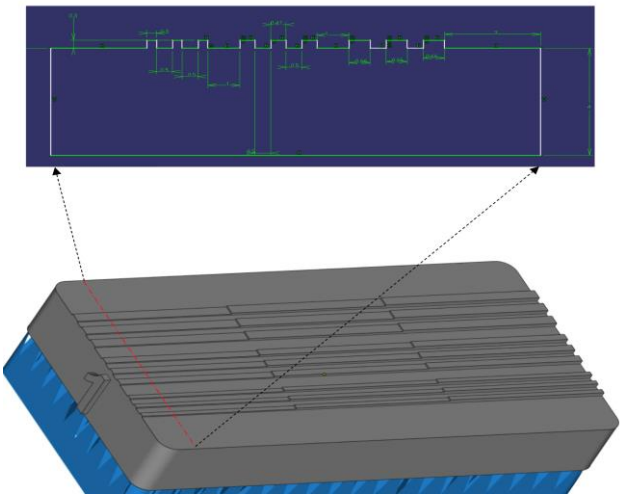

Figure 4: Sample CAD Design

The data characterization process involved scanning each feature using a Sensofar Smart 3D profiler with a 10x magnification lens and generating 3D surface profiles. Two-dimensional profiles were extracted from each 3D profiles, and the measured points were averaged, and their standard deviations calculated.

4.4. Results Summary for Continuous Laser Samples

Figure 5 shows 54 bars with standard deviations plotted for Case 1-3 for all six samples. Case 1 (C1) had the highest mean percentage error (37.72%) the lowest was calculated for Case 3 (3.72%). Cases 2 and 3 had errors ranging from 3.72% to 17%, which is better than Case 1, but still has room for improvement. The theoretical model always underestimated the minimum feature size, with the highest MPE in Case 1 and the lowest varying between Cases 2 and 3. The potential underestimation of power, hatch spacing, and speed parameters needs further investigation as they affect the melt-pool size and feature width. The study aims to improve the analytical prediction by tuning the current model to predict the actual width more accurately.

5. New Tunable Feature Width prediction Model

5.1. Model modified using Optimised Coefficients

The Rosenthal equation and hatch spacing were used to predict the theoretical feature width for Case 1, 2 and 3. This is summarised in equations 1-3. The parameters that can be varied in this equation are power, speed and hatch spacing. Layer height may be varied as well as a function of the build height. There was relatively poor width prediction accuracy compared with the experimental results. Thus, it is proposed to improve the model to facilitate its tunning, using real experiment by enabling modification of the influence of machine parameters (power, speed, hatch spacing and layer height) on the predicted widths. This can be achieved by multiplying these parameters with coefficients that can be optimised based on the widths measured experimentally.

The following modifications were made for the following:

Case 1 and 2:

$$\boldsymbol{w_{theo\_p} = \left(\sqrt{\frac{8}{\pi e}\cdot\frac{\lambda.Cf_p.P}{Cf_s.\rho.C_p.v(T_m-T_o)}}\right) + Cf_h.h_i + Cf_{Lh}.Lh} \quad (6)$$

Case 3:

$$\boldsymbol{w_{theo\_p} = \left(\sqrt{\frac{8}{\pi e}\cdot\frac{\lambda.Cf_p.P}{Cf_s.\rho.C_p.v(T_m-T_o)}}\right) + Cf_h.2h_{c.i} + Cf_{Lh}.Lh} \quad (7)$$

Where $\boldsymbol{Cf_p, Cf_s, Cf_h \text{ and } Cf_{Lh}}$ refer to the coefficient of power, speed, hatch spacing and layer height respectively.
The algorithm chosen for the optimisation process is the L-BFGS-B algorithm. This was selected because it is well established and easy to apply with specific boundaries [8]. The optimisation algorithm was run to determine which coefficients $\boldsymbol{Cf_p, Cf_s, Cf_h \text{ and } Cf_{Lh}}$ returned the best results. The boundaries selected for $\boldsymbol{Cf_p, Cf_s}$, were 0.1,10 to avoids negative square root for w_{theo_p} calculation. In addition, the boundaries for layer height were specified as -10:10 because there might be a negative error due to the melting and solidification of metallic powder for the final layer, unevenness of the build surface layer and thermal shrinkage.

Figure 6 shows the results from the first optimisation process using all LPBF continuous laser data for samples 1-6. The MPE for all cases varies between 2 and 15%, which is a significant improvement from the previous MPE range of 3-37.2% from the original model. However, this may be due to overfitting the data, which may not guarantee the prediction accuracy outside of the experimental space provided by the tuning process. Therefore, the model was tuned to a single sample data in order to use the other 5 samples as validating sets for the obtained coefficients.

Table 3. Summary of coefficients from LBFG Optimisation algorithm

Laser Type	Tuning Data				
		Power	Speed	Hatch Spacing	Layer Height
C.L (AlSi7Mg)	Samples 1-6	1.360	0.683	0.266	0.10
C.L (AlSi7Mg)	Samples 1	1.383	0.598	0.182	0.01

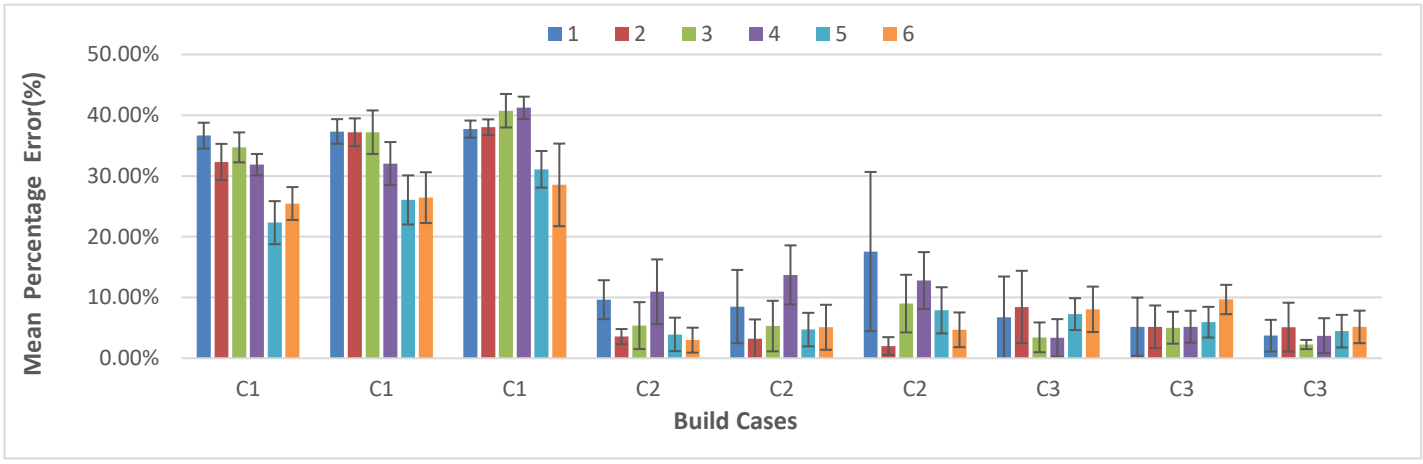

Figure 6. Plot of Mean Percentage Error (MPE) and standard deviations for samples 1-6. Where C1, C2, C3 represent Case 1, Case2, Case 3

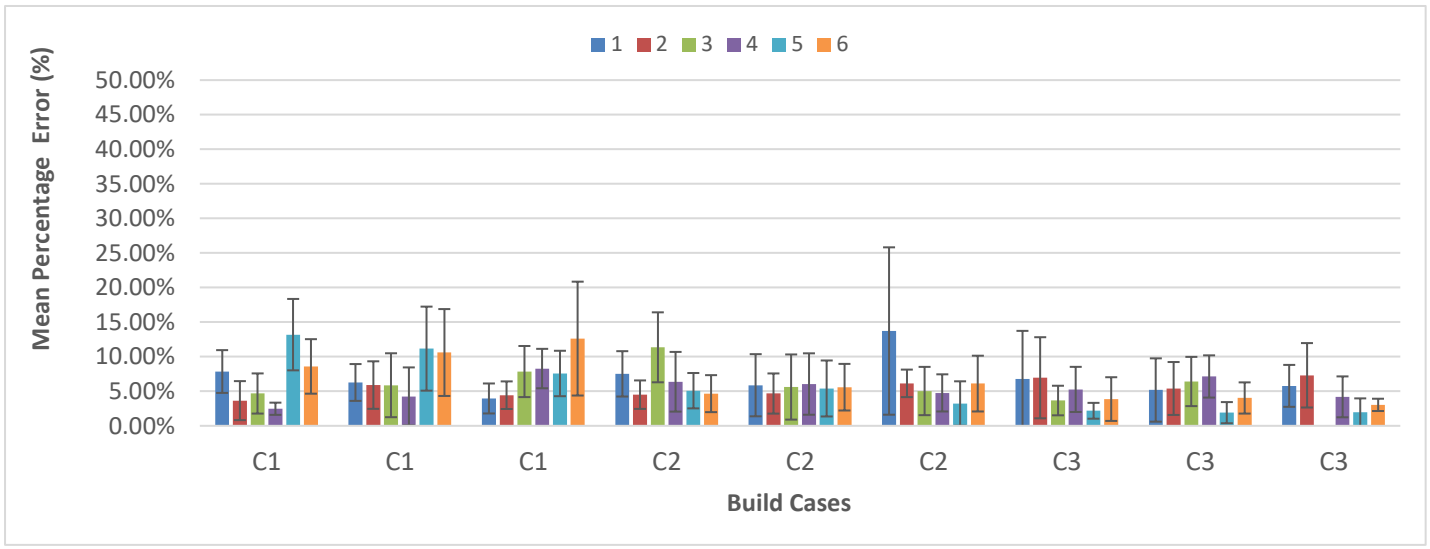

Figure 5. Plot of Mean Percentage Error (MPE) & standard deviations for samples 1-6 tuned to all data. Where C1, C2, C3 represent Case 1, Case2, Case 3

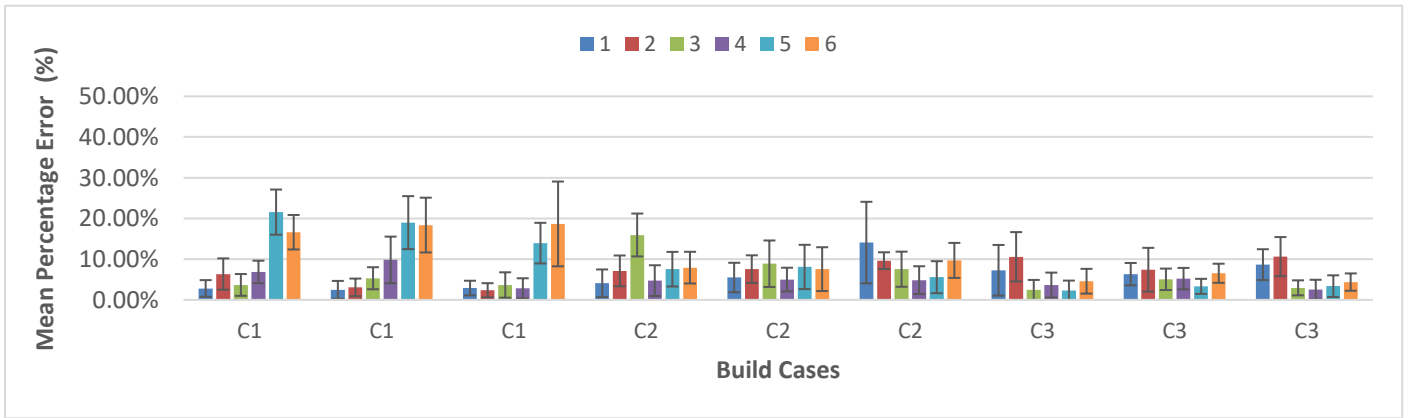

Figure 8. Plot of MPE for Samples 1-6 tuned to sample 1 data. Where C1, C2, C3 represent Case 1, Case2, Case 3.

5.2. Model tuning to single sample experimental set

In this second optimisation, only the data from sample 1 was used to optimise the coefficients of the new model. A comparison of the MPE for the optimisation based on all sample data to sample 1 data is shown in Figure 8.
In general, the MPE after optimisation with one sample data ranges from approximately 2-20%, which is 7% larger than the MPE after optimisation with all sample data which ranges from about 2-13%, and it is still a significant improvement from the original model whose prediction error ranged from about 3.72-37.72%. In the context of a millimetre scale feature designed at 0.4mm. This 20% MPE value (from single sample optimisation) translates to a maximum error of ± 0.08mm, which can be considered acceptable at this scale.

6. Discussion

In this paper, we assumed that the Rosenthal equation could predict melt-pool width and determine minimum feature width for different scenarios. Six AlSi7Mg samples were made and compared to theoretical calculations, which under-estimated the feature width. Further testing showed that process parameters were not being fully considered, leading to an attempt to optimize them using an L-BFG algorithm.

Following L-BFG optimization of Power, Speed, Hatch Spacing, and Layer height, the resulting coefficients were summarized in Table 3. The optimized power coefficient was consistently greater than one, suggesting that the effect of power was underestimated for AlSi7Mg. One possible explanation for this is the laser absorptivity parameter, which is a material thermo-physical property experimentally derived from published literature by Tang et al. [2]. The published literature reports an absorptivity range of 0.32 to 0.39 for AlSi10Mg, with an average of 0.33 used to calculate melt-pool width. As the laser power used in the AlSi7Mg experimentation was higher than the published literature (360W), the absorptivity likely increased, making the extra average of 30% power compensation logical.

The optimised coefficients of speed were consistently less than one for AlSi7Mg, indicating an overestimation of speed's impact on melt-pool width. This results in larger melt-pool widths than previously predicted since the analytical calculation of the melt-pool width is inversely proportional to the square root of the speed. For continuous laser, the low influence of hatch spacing may be due to the laser's continuous power and speed along each scan, hence only the hatch spacing between adjacent melt-pools needs to be compensated for.
The coefficient of layer height is always less than 0.1 indicating that it has little effect on the melt-pool width.

7. Conclusion

In this paper, an analytical model was developed and optimized to determine the minimum feature width of machine/material combination. The Rosenthal equation was used to estimate the melt-pool width and input data required by the model included power, speed, hatch spacing, layer height, and material properties. The original model prediction under-estimated feature widths, so L-BFG optimization was used to tune the model for higher accuracy. The optimized model can predict minimum feature width for AlSi7Mg (SLM280) material (machine) combination with a single sample.
The results are promising for the AlSi7Mg material and SLM280 machine, hence future work will involve validating the methodology with a different combination of material and machine to evaluate if the proposed model could indeed become a generic model.

8. References

[1] P. Promoppatum, S. C. Yao, P. C. Pistorius, and A. D. Rollett, “A Comprehensive Comparison of the Analytical and Numerical Prediction of the Thermal History and Solidification Microstructure of Inconel 718 Products Made by Laser Powder-Bed Fusion,” *Engineering*, vol. 3, no. 5, pp. 685–694, 2017, doi: 10.1016/J.ENG.2017.05.023.

[2] M. Tang, P. C. Pistorius, and J. L. Beuth, “Prediction of lack-of-fusion porosity for powder bed fusion,” *Addit. Manuf.*, vol. 14, pp. 39–48, 2017, doi: 10.1016/j.addma.2016.12.001.

[3] J. Metelkova, Y. Kinds, K. Kempen, C. de Formanoir, A. Witvrouw, and B. Van Hooreweder, “On the influence of laser defocusing in Selective Laser Melting of 316L,” *Addit. Manuf.*, vol. 23, no. August, pp. 161–169, 2018, doi: 10.1016/j.addma.2018.08.006.

[4] L. Zhang, H. Zhu, S. Zhang, G. Wang, and X. Zeng, “Fabricating high dimensional accuracy LPBFed Ti6Al4V part by using bi-parameter method,” *Optics and Laser Technology*, vol. 117. pp. 79–86, 2019, doi: 10.1016/j.optlastec.2019.04.009.

[5] J. Kim, S. Ji, Y.-S. Yun, and J.-S. Yeo, “A Review: Melt Pool Analysis for Selective Laser Melting with Continuous Wave and Pulse Width Modulated Lasers,” *Appl. Sci. Converg. Technol.*, vol. 27, no. 6, pp. 113–119, 2018, doi: 10.5757/asct.2018.27.6.113.

[6] MSE Supplies LLC, “AlSi7Mg Aluminum Based Metal Powder for Additive Manufacturing (3D Printing),” 2022. [Online]. Available: https://www.msesupplies.com/en-gb/products/alsi7mg-aluminum-based-metal-powder-for-additive-manufacturing-3d-printing. [Accessed: 10-Oct-2022].

[7] G. Galimberti, E. L. Doubrovski, J. C. Verlinden, B. Previtali, and M. Guagliano, “Investigating the Links between Process Parameters and Their Influence on the Aesthetic Evaluation of Selective Laser Melted Parts 1,” *Proc. 27th Annu. Int. Solid Free. Fabr. Symp.*, no. November, pp. 2367–2386, 2016.

[8] R. H. Byrd, P. Lu, J. Nocedal, and C. Zhu, “A Limited Memory Algorithm for Bound Constrained Optimization,” *SIAM J. Sci. Comput.*, vol. 16, no. 5, pp. 1190–1208, 1995, doi: 10.1137/0916069.